# Mechanism of p300 Specific Histone Acetyltransferase Inhibition by Small Molecules

M. Arif,[†] Suman Kalyan Pradhan,[‡] Thanuja G R,[†] B. M. Vedamurthy,[†] Shipra Agrawal,[§] Dipak Dasgupta,[‡] and Tapas K. Kundu*,[†]

*Transcription and Disease Laboratory, Molecular Biology and Genetics Unit, Jawaharlal Nehru Centre for Advanced Scientific Research, Jakkur, Bangalore 560064, India, Biophysics Division, I/AF, Saha Institute of Nuclear Physics, Bidhannagar, Kolkata 700064, India, and Institute of Bioinformatics and Applied Biotechnology, International Technology Park Bangalore (ITPB), Whitefield Road, Bangalore 560066, India*

*Received June 1, 2008*

Dysfunction of histone acetyltransferases (HATs) leads to several diseases including cancer, diabetes, and asthma. Therefore, small molecule inhibitors and activators of HATs are being considered as new generation therapeutics. Here, we report the molecular mechanisms of p300 HAT inhibition by specific and nonspecific HAT inhibitors: garcinol, isogarcinol, and **1** (LTK14). The p300 specific HAT inhibitor **1** behaves as a noncompetitive inhibitor for both acetyl-CoA and histone, unlike nonspecific HAT inhibitors garcinol and isogarcinol. The isothermal calorimetric data suggest that there is a high affinity enthalpy driven single binding site for **1** on p300HAT domain in contrast to two binding sites for garcinol and isogarcinol. Furthermore, the precise nature of molecular interactions was determined by using fluorescence, docking, and mutational studies. On the basis of these observations, we have proposed the mechanisms of specific versus nonspecific HAT inhibition by these small molecule compounds, which may be useful to design therapeutically favorable HAT inhibitors.

## Introduction

Chromatin is a highly dynamic entity present in the nucleus of eukaryotic cells. It is the physiological template for all the nuclear related processes like transcription, replication, recombination, chromosomal segregation, and repair. The structural unit of chromatin, the nucleosome, encompasses ∼147 bp of DNA wrapped around an octamer of core histone proteins (two copies each of H2A, H2B H3 and H4) in ∼1.7 turns.[1] The dynamic interconversion of chromatin between transcriptionally active euchromatin and transcriptionally repressed heterochromatin plays an important role in transcription regulation.[2] It has been shown that the establishment of distinct chromatin region can be achieved through specific covalent modification of histones (e.g., acetylation, methylation, and phosphorylation),[3,4] through nucleosome assembly with histone variants (e.g., H2A.Z, CENPA), or with the help of nucleosome binding nonhistone proteins (e.g., HP1, PARP-1, and PC4).[5]

Post-translational modifications of chromatin play a key role in the regulation of gene expression, cell growth, and differentiation.[3,4] Among different histone modifying enzymes, histone acetyltransferases (HATs[a]) and histone deacetylases (HDACs) affect the acetylation of histones and nonhistone proteins, thereby affecting the downstream biological functions. Recent evidence has shown that altered HAT and HDAC activities may lead to several diseases, ranging from cancer to neurodegenerative disorders.[6−9]

The histone acetyltransferase p300 is the most thoroughly studied among different HAT families. It is a highly potent enzyme that acetylates histones and several other proteins (factor acetyltransferase, FAT).[10,11] Mechanistically, p300 acts as a transcriptional coactivator through the direct interaction with a diverse set of transcription factors and RNA polymerase II transcription machinery.[12] The intrinsic HAT activity of p300 plays an important role in the transcriptional coactivation of CREB, c-Jun, c-Fos, c-Myb, p53, Stats, nuclear receptors, RelA GATA, p73, etc.[7,10,13,14]

A proper balance of acetylation and deacetylation is important for the normal cellular growth and differentiation. Therefore, dysfunction of p300 has been implicated in diseases like inflammatory processes, Huntington disease, cardiac diseases, diabetes mellitus, AIDS, and cancer.[5,14,15] These observations lead to consideration of small molecule modulators (activators and inhibitors) of p300 as potential new generation therapeutics. These small molecule compounds would also be highly useful for probing the functional significance of the histone acetyltransferase activity in vivo.

Recently, a few successful attempts have been made to understand the mechanisms of p300 mediated acetylation of histones,[16−18] including the cocrystal structure of p300 HAT domain and p300 specific, synthetic inhibitor Lys-CoA. It has been shown that p300 follows an unusual the hit-and-run (Theorell−Chance) mechanism of enzyme action.[19] p300 gets extensively autoacetylated in an intermolecular fashion, which is highly cooperative in nature.[18] Autoacetylation of multiple lysines at the proteolytic sensitive loop was found to be important for the regulation of its catalytic activity.[17] Presumably, the distal protein contacts or a particular loop conformation may influence p300 autoacetylation.[20] Autoacetylation of p300 is closely linked to the p300 mediated transcriptional regulation.[17] The acetylation of p300 is essential to initiate the transcription. It was predicted that the autoacetylated p300 gains a favorable structural change to dissociate from the transcriptional preinitiation complex (PIC), leading to initiation of activator dependent transcription.[21] By employing surface enhanced raman spectroscopy (SERS), we have shown that indeed the autoacetylation of p300 induces a significant structural alteration in the p300HAT domain.[22]

* To whom correspondence should be addressed. Phone: (0091) 80-2208-2840. Fax: (0091) 80- 22082766. E-mail: tapas@jncasr.ac.in.

[†] Jawaharlal Nehru Centre for Advanced Scientific Research.

[‡] Saha Institute of Nuclear Physics.

[§] Institute of Bioinformatics and Applied Biotechnology.

[a] Abbreviations: HAT, histone acetyltransferase; HDAC, histone deacetylase; p300HD, p300 histone acetyltransferase domain; IG, isogarcinol.

10.1021/jm800657z CCC: $40.75 
Published on Web 12/16/2008

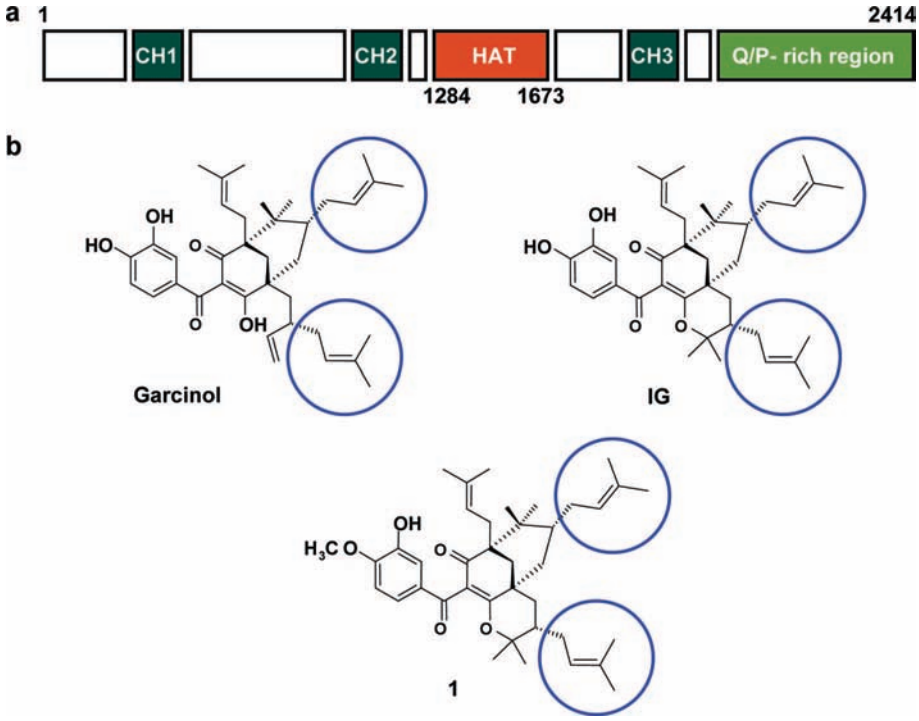


**Figure 1.** (a) Schematic representation of p300 domain structure. The functional domains of p300 include CH1, CH2, CH3, HAT domain, and Q/P-rich region. Note that the p300 HAT domain used in this work encompasses amino acid residues 1284−1673 as shown. (b) Chemical structures of garcinol, IG, and **1**. The blue circled moieties represent the region of structural difference between garcinol and the other two inhibitors (IG and **1**) in their three-dimensional orientations.

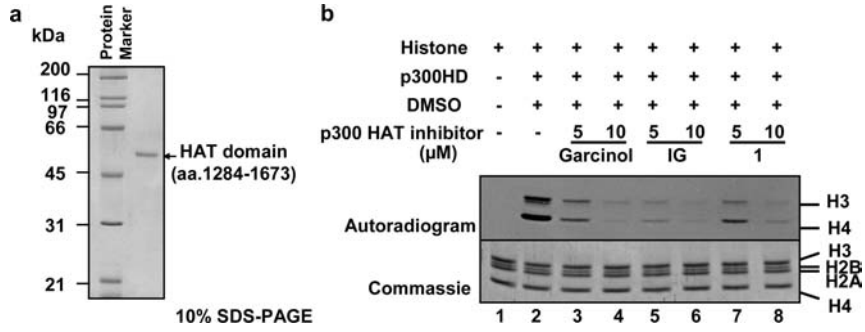


**Figure 2.** (a) Purification profile of recombinant p300 HAT domain (p300HD) (aa 1284−1673). (b) Garcinol derivatives inhibit p300 HAT domain. HAT assays were performed by using highly purified HeLa core histones in the absence (lane 1) and presence of solvent control DMSO (lane 2). Also shown are results of histone with HAT in the presence of garcinol (lanes 3 and 4), IG (lanes 5 and 6), and **1** (lanes 7 and 8) at 5 and 10 $\mu$M concentrations, respectively.

Previously, we have shown that the polyisoprenylated benzophenone, garcinol (Figure 1b), isolated from *Garcinia indica* (an edible fruit), is a potent nonspecific inhibitor of histone acetyltransferase p300.[23] In order to find out more potent, specific, and less toxic inhibitors, we synthesized several garcinol derivatives based on isogarcinol (IG), a product of intramolecular cyclization of garcinol (Figure 1b). IG was also found to be a nonspecific inhibitor of HATs.[24] Remarkably, with a monosubstitution at the C-14 position, **1** (LTK14)[24] (Figure 1b) converted the IG to a highly specific inhibitor of p300 HAT activity. IG and **1** are characterized by the presence of a lactone ring. Furthermore, **1** was shown to inhibit HIV multiplication in SupT1 cells by inhibiting histone acetylation and hence has the potential to be a lead molecule for therapeutics.[24] The significant alteration in the specificity has led us to investigate the molecular mechanism responsible for the differential nature of HAT inhibition by these structurally close related inhibitors (Figure 1b and Supporting Information Figure 1). Since it is difficult to obtain highly purified full length p300 (p300fl) from eukaryotic expression systems in sufficient amounts for biocalorimetry and other biophysical studies, we have used p300 HAT domain (p300HD) (1284−1673aa) (Figure 1a) in the present studies. Recombinant p300HD was overexpressed upon co-transformation of human histone deacetylase SirT2 with a p300HD construct and purified from *E.coli* (Figure 2a). It is pertinent to point out that mechanistic and substrate selectivity parameters for p300fl and those of p300HD were reported to be quite similar, which justifies our choice of p300HD in the present studies.[16,17] We believe that this is the first report that attempts to throw light on the molecular mechanism of differential nature of the inhibition of p300 HAT brought about by nonspecific (e.g., garcinol and IG) and specific (e.g., **1**) inhibitors of natural origin.

## Results and Discussion

**p300 HAT Domain as Target of Garcinol Derivatives.** The dose dependent inhibition of the p300HD HAT activity by different inhibitors was investigated by gel fluorography/

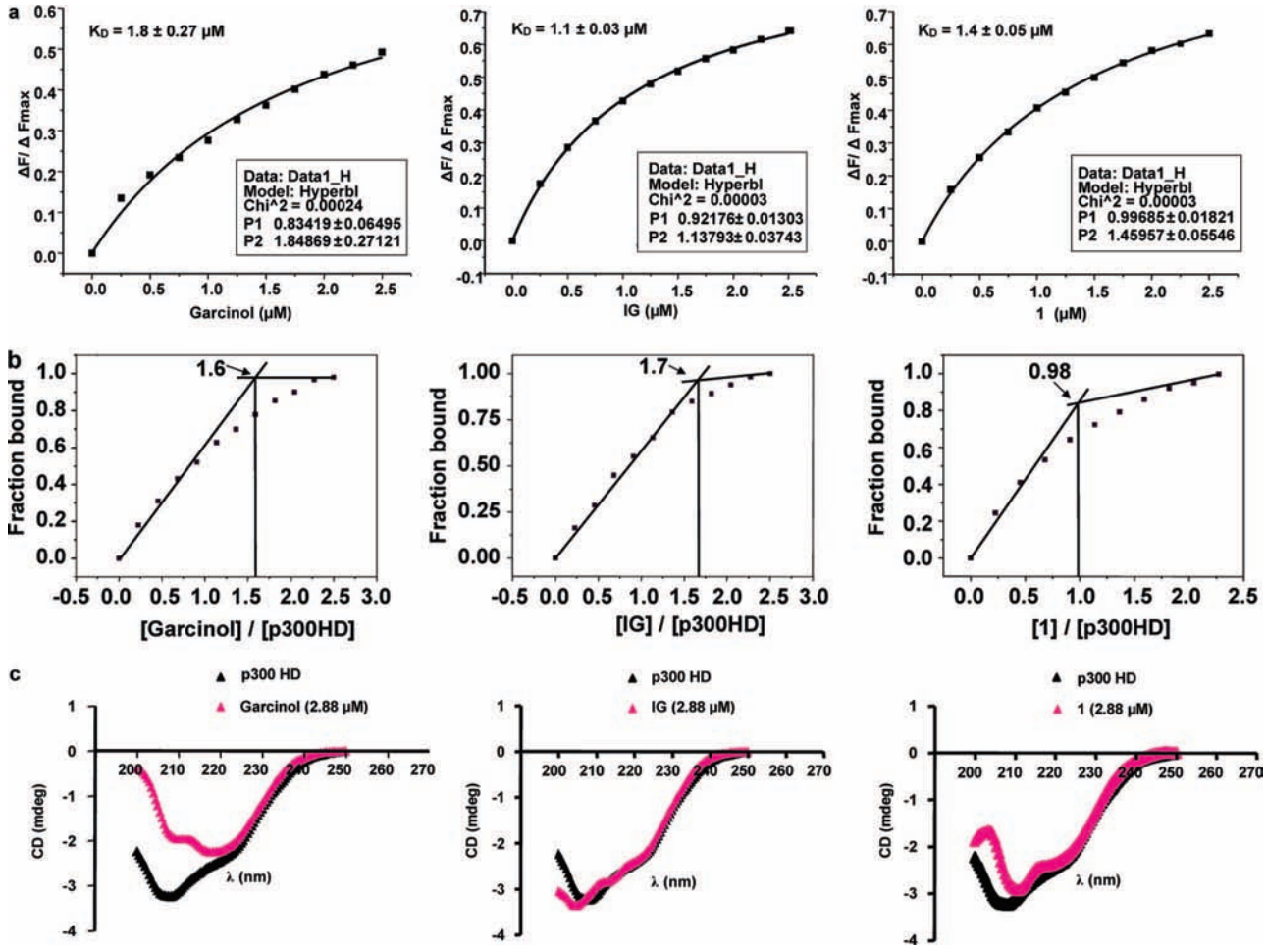


**Figure 3.** (a) Curve fitting analysis to evaluate the dissociation constant for the association of the different HATi with p300 HAT domain (p300HD): (left) garcinol, (middle) IG, and (right) **1**. The concentration of the protein was 1.2 $\mu$M in all the three cases. $K_d$ values obtained from the nonlinear least-squares method are 1.8, 1.1, and 1.4 $\mu$M for garcinol, IG, and **1**, respectively. (b) Method to determine binding stoichiometry associated with the binding of ligands with p300 HAT domain. The abscissa values corresponding to the intersection of the two straight lines for garcinol, IG, and **1** are 1.6, 1.7, and 0.98, respectively. (c) Far-UV CD spectra of 2.88 $\mu$M of different HAT inhibitors and in the presence of 1.2 $\mu$M p300HD in buffer at 25 °C. Left, middle, and right plots correspond to garcinol, IG, and **1**, respectively. The black spectra denote the p300HD alone in all cases. The spectra were recorded over the wavelength range shown.

autoradiography assay. Figure 2b represents the profile of HAT activity in the presence of the three inhibitors. Results show that all three ligands, garcinol, IG, and **1**, inhibit the HAT activity of p300HD in a concentration dependent manner (compare lane 2 vs lanes 3 and 4, vs lanes 5 and 6, and vs lanes 7 and 8 of Figure 2b). A similar degree of inhibition was also observed for p300fl[23,24] (data not shown). Taken together, these results suggest that the inhibition of p300fl is executed through the direct inhibition of p300HD HAT activity which could be the direct target of the p300 HAT inhibitors. These results justify the use of p300HD as the appropriate model to understand the molecular basis of the inhibition of the HAT activity of p300fl by these small molecules. Hence, we carried out biophysical and kinetic studies with p300HD to understand the mechanism of p300 inhibition.

**In Vitro Characterization of p300 HAT Inhibitors Interaction with the p300HD.** The nature of binding of p300HD with the different HAT inhibitors were estimated from the ligand concentration dependent decrease in fluorescence emission (at 340 nm) of the protein. The resulting binding curves suggest a noncooperative mode of binding. Dissociation constants were found to be 1.8 ± 0.27, 1.1 ± 0.03, and 1.4 ± 0.05 $\mu$M for garcinol, IG, and **1**, respectively (Figure 3a). The dissociation constant values are in the same range (micromolar) necessary for the inhibition of HAT activity. Furthermore, they fall in the same range for the $IC_{50}$ values reported for these ligands with PCAF and p300.[23,24] Binding stoichiometry was also estimated from the intersection of the two straight lines of a least-squares fit plot of the normalized decrease in fluorescence against the ratio of input concentrations of the respective ligand and the p300 HAT domain.[25] The abscissa values corresponding to the intersection of the two straight lines for garcinol, IG, and **1** are 1.6, 1.7, and 0.98, respectively (Figure 3b).

**Table 1.** Modified Stern−Volmer Plot for the Acrylamide Quenching of p300HD Alone and after Preincubation with Different HAT Inhibitors

| system | $K_{sv}$ ($M^{-1}$) | % accessibility ($1/f_e$) |
|---|---|---|
| control HAT (1.2 $\mu$M) | 21.9 ± 0.3 | 80 ± 1.2 |
| HAT (1.2 $\mu$M) + garcinol (2.5 $\mu$M) | 15 ± 0.5 | 78 ± 1.1 |
| HAT (1.2 $\mu$M) + IG (2.5 $\mu$M) | 16.3 ± 0.7 | 75 ± 1 |
| HAT (1.2 $\mu$M) + **1** (2.5 $\mu$M) | 15.8 ± 0.9 | 67 ± 2 |

Acrylamide quenching of tryptophan fluorescence of the protein was used to detect the ligand-induced alteration in the tertiary structure of the protein, if any. Tryptophan accessibility and Stern−Volmer constants of the free and ligand-bound protein (summarized in Table 1; for plot, see Supporting Information Figure S2) were estimated from modified Stern−Volmer

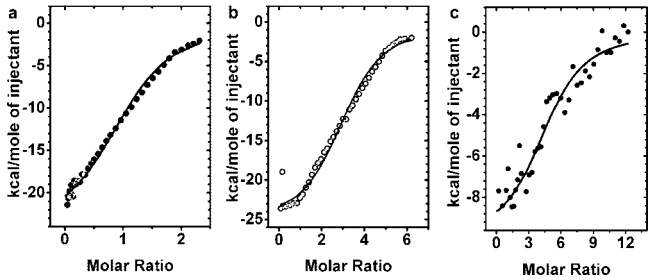


**Figure 4.** Calorimetric titration of different HAT inhibitors with p300HD. Parts a, b, and c show the integrated heat change for the corresponding injections along with one set of sites-binding model fit of garcinol, IG, and **1** with p300HD at 20 °C, respectively.

**Table 2.** Thermodynamic Parameters for the Interaction of HAT Inhibitors with p300HD

| system | $N$ | $K_d$ ($\mu$M) | $\Delta G$ (kcal/mol) | $\Delta H$ (kcal/mol) | $\Delta S$ (eu) |
|---|---|---|---|---|---|
| HAT + garcinol | $1.87 \pm 0.06$ | $6.6 \pm 0.2$ | $-7.03 \pm 0.15$ | $-21.1 \pm 0.89$ | $-48.2 \pm 1.25$ |
| HAT + IG | $2.1 \pm 0.09$ | $5.9 \pm 0.1$ | $-7.8 \pm 0.09$ | $-23 \pm 0.95$ | $-57.9 \pm 1.65$ |
| HAT + **1** | $1.08 \pm 0.08$ | $9.1 \pm 0.2$ | $-6.3 \pm 0.10$ | $-18.2 \pm 0.98$ | $-37.7 \pm 1.23$ |

plots.[26] Results suggest that the change in accessibility is significant upon addition of **1** (Table 1). The alteration in the accessibility value originates from the ligand-induced change in the tertiary structure of the protein. It may be suggested that the association of the other two ligands does not lead to a major alteration in the tertiary structure of the protein. The extent of change, however, does not suggest any radical alteration of the tertiary structure for p300HD even in case of **1**. On the other hand, we noticed a change in the secondary structure of p300HD upon interaction with garcinol and **1** from far-UV CD (200−250nm). Results are shown in Figure 3c. The shape of the CD spectrum of the protein suggests a preponderance of $\beta$-sheet in the protein. Addition of garcinol and **1** changes the secondary structure, which results in alteration of the shape in the CD spectra though not to a major extent. The change is not marked in the case of IG. Earlier reports have shown that the specific and nonspecific inhibitors of p300 bind to the amide groups of a helix and thereby differentially alter the enzyme structure. Present data are consistent with earlier reports from ligand-induced alteration of SERS for the p300fl.[24] It is mentioned that CD spectra of p300HD in the presence of the ligands were monitored under nonsaturating concentrations of the ligands because of the presence of DMSO solvent necessary for solubilizing the ligands. It also prevented us from monitoring the CD spectra of the protein beyond 200 nm. Therefore, we refrained from any quantitive estimation of the relative percentages of the secondary structure because all available programs require CD data up to 190 nm.

**Isothermal Titration Calorimetry (ITC) Studies of the HAT Inhibitors with p300HD.** In order to have insights regarding the molecular nature of the interaction between the inhibitors and the protein, isothermal titration calorimetry was performed. Representative binding isotherms for all three are shown in Figure 4, and the results are summarized in Table 2. Dissociation constants agree to a reasonable degree with the value obtained from the fluorescence method. In addition to the associated thermodynamic parameters, isothermal titration calorimetry indicated an important difference in the binding modes for garcinol, IG, and **1**. It is clear from Table 2 that only one molecule of **1** binds to the p300HD. In contrast, two molecules of garcinol and IG bind to the protein. These results are consistent with the stoichiometry obtained from the fluorescence titration curve obtained from the progressive addition of the ligands to the protein (Figure 3b). The affinity constant values could be grouped similarly into two classes. Garcinol and IG have relatively higher affinity than **1**. All interactions are enthalpy driven. It implies that the complex formation takes place because of enthalpy driven noncovalent interactions like H-bonding and/or stacking interactions. This is partially compensated by a negative entropy change. The unusually high negative value of $\Delta H$ in the range 18−22 kcal/mol for garcinol and IG (Table 2) could be ascribed to the following parsing of enthalpy: $\Delta H_{total} = \Delta H_{site1} + \Delta H_{site2}$, the subscripts referring to the enthalpy change associated with the first and second binding site, respectively. A similar explanation could also account for the high negative entropy change. In the reported crystal structure of the complex of PCAF HAT domain and acetyl-CoA, multiple hydrogen bonds have been observed to stabilize the association.[27] Large values of negative entropy changes might originate from the ordering of water molecules at the protein−ligand binding interface. As reported in the crystal structure of a ternary complex, the HAT domain of tetrahymena GCN5 (tGCN5) bound with its physiologically relevant ligands[28] coenzyme A (Co A) and a histone H3 peptide, water mediated hydrogen bonds are a potential source of localization of water molecule. Conformational change of the small ligands, another potential source of negative entropy, could also be possible. In terms of the enthalpy and entropy changes, **1** exhibits a difference from garcinol and IG. The lower value of enthalpy change in this case could be ascribed to the absence of two binding sites. Relatively lower value of negative entropy change also characterizes the **1** and protein association.

**Kinetic Characterization of the Mode of Inhibition of p300 HAT Inhibitors.** In order to further understand the nature as well as the mechanism of inhibition, reversibility of the ligand binding was established by equilibrium dialysis and dilution experiments (data not shown). We then compared the inhibition kinetics of p300HD HAT activity by the three ligands for both substrates acetyl-CoA and core histone. Double-reciprocal plots were constructed to find the nature of inhibition. Results are summarized in Figure 5. Inhibition kinetics studies clearly demonstrate the difference in the mechanism of inhibition caused by specific (**1**) and nonspecific (garcinol and IG) inhibitors. They show that the inhibition patterns for the garcinol and IG are similar. Both of them show competitive inhibition for the acetyl-CoA binding site on p300HD and noncompetitive inhibition for the histone binding site (Figure 5, parts a and b, respectively). In contrast, **1** was found to be a noncompetitive inhibitor for both acetyl-CoA and histone binding sites (Figure 5c), which is consistent with the earlier report with p300fl.[24] These difference in the nature of inhibition could be attributed to the chemical modifications in **1** (compare structures of Figure 1b). It is noted that the three-dimensional (3D) structures of IG and **1** are very similar (Supporting Information Figure S1). Further, the inhibitor constant ($K_i$) values for all the three inhibitors were determined using the slope and the intercept replots obtained from the primary plots. $K_i$ values for garcinol, IG, and **1** are $4.9 \pm 0.2$, $3.9 \pm 0.2$, and $5.1 \pm 0.3$ $\mu$M, respectively. The observed $K_i$ values are in the similar range (micromolar) of $K_d$ values determined from the ITC and the fluorescence titration results (Table 2 and Figure 3a). These are also in the same range (micromolar) necessary for the inhibition of HAT activity.

**Mechanism of Inhibition of p300HD with Garcinol Derivatives.** On the basis of the data obtained from thermodynamic studies and inhibition kinetic studies, we proposed a mechanism (Scheme 1) of inhibition by both specific and nonspecific inhibitors. Isothermal calorimetric titration yields a binding

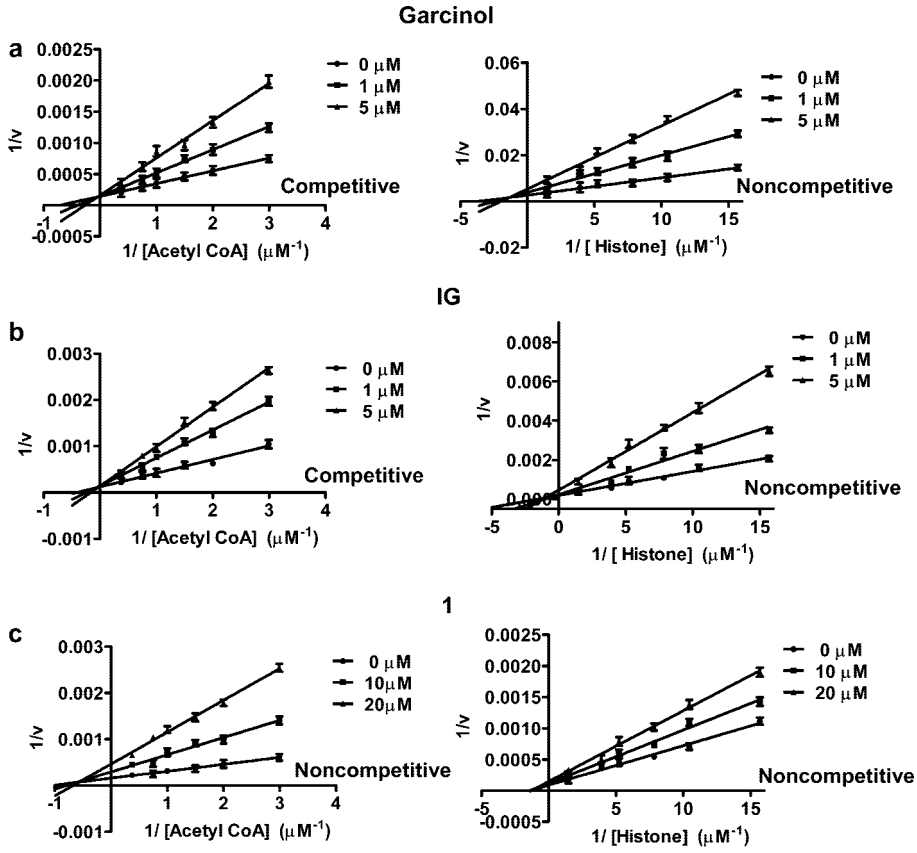


**Figure 5.** Inhibition kinetics of garcinol, IG, and **1** with p300HD. Lineweaver−Burk plots for garcinol, IG, and **1** are shown in parts a, b, and c, respectively. Each experiment was performed three times, and reproducibility was within 15%.

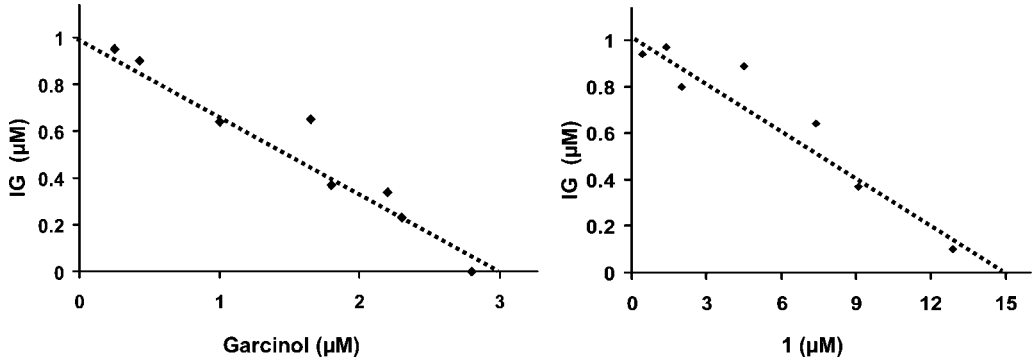


**Figure 6.** Isobologram analyses of IG versus garcinol (left) and of IG versus **1** (right) are shown. The experimental data are best fit to the theoretical line of additivity (dashed line).

stochiometry of 2 for both garcinol and IG per molecule of the enzyme. Out of these two, at least one molecule binds to the acetyl-CoA binding site (Scheme 1, part a.1), since these inhibitors exhibit a competitive mode of inhibition in the presence of an excess of histones. The other binding site would be a site other than a histone binding site (Scheme 1, part a.2) because these inhibitors exhibit a noncompetitive mode of inhibition in the presence of excess acetyl-CoA. However, the remote possibility of the second molecule binding to structurally altered p300HD under the influence of substrate(s) binding cannot be excluded. In contrast, **1**, which shows 1:1 stochiometry of binding, neither binds to histone binding site nor to acetyl-CoA binding site (Scheme 1, parts b.1 and b.2), as the ligand exhibits a noncompetitive mode of inhibition toward both substrates. It is apparent that conversion of the phenolic hydroxyl group at C-14 to a methoxy group (a bulky group) in **1** has led to the reduction in its binding stochiometry for p300HD. In

**Scheme 1.** Proposed Mechanism of Inhibition of p300HD with Garcinol, IG, and **1**

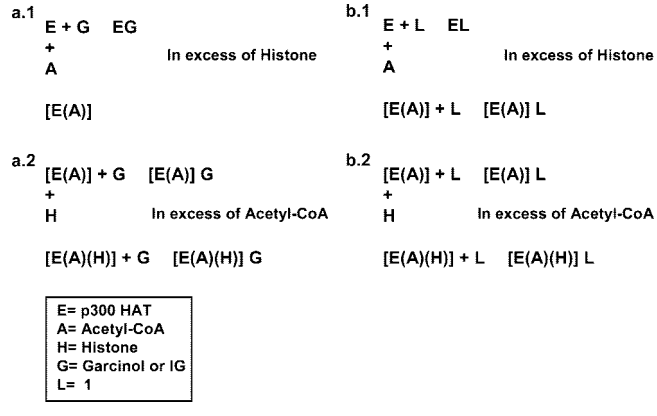

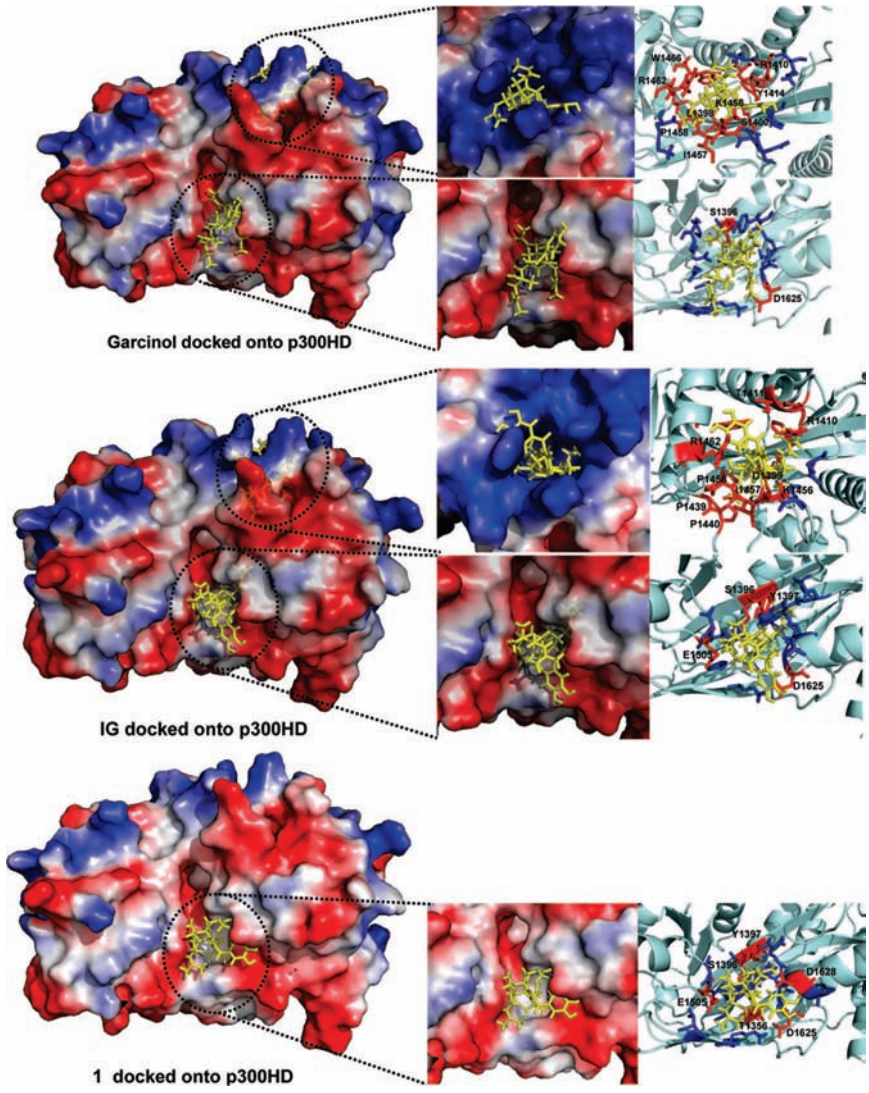


**Figure 7.** The crystal structure of p300HD (PDB code 3BIY) is used to dock the HAT inhibitors using HEX 4.5 software. Top, middle, and bottom rows represent the p300HD−garcinol complex, the p300HD−IG complex, and the p300HD−**1** complex, respectively. The ligand is shown in yellow stick figure representation, whereas the protein is shown with surface electrostatic potential as generated by PyMol.[34] Respective blow-up images are shown on the right-hand side in both surface electrostatic potential and in cartoon form, where the top blow-up image is of acetyl-CoA active site and the bottom is for the second binding site (see Supporting Information Table 1 for the amino acid residue labeling).

addition, the comparison of the inhibition kinetics pattern suggests that unlike garcinol and IG, **1** does not bind to the acetyl-CoA binding site in the p300HD. It implies that −OH at the C-13 and C-14 positions in garcinol and IG would have a role in binding to the acetyl-CoA binding site of the p300HD, since both of them compete for the acetyl-CoA binding site. Similarly, the bulky group at the C-14 position of **1** may be an unfavorable structural choice that could not be accommodated and hence cannot bind to the acetyl-CoA binding site because of probable steric hindrances. It is noted that the 3D structures of IG and **1** are very similar (Supporting Information Figure S1). Therefore, it suggests that there exists a strict structural requirement for the interacting ligand (i.e., inhibitor in the given case) to the acetyl-CoA binding site. This is further supported by the fact that a strict structural requirement exists at the ADP-ribose portion of Lys-CoA where the adenosine ring exists in a well ordered form.[19] This is supported by the fact that the entropy is relatively lower in the case of garcinol and IG than **1** (Table 2), which is a reflection of the proposed strict structural requirement at the acetyl-CoA binding site.[19] At the same time it is noticed that there is a difference of −3 to −5 kcal/mol binding enthalpy between the two classes of ligands (Table 2). The value is equivalent to the enthalpy required for the formation of an H-bond. It is therefore rational to propose that the −OH groups at C-13 and C-14 in garcinol and IG play a key role in binding to the acetyl-CoA binding site via H-bonding with the appropriate amino acid side chain or peptide backbone of p300HD in the vicinity of acetyl-CoA binding site (Figure 7 and Supporting Information Table 1). Such interactions along with the structural complementarity to the acetyl-CoA binding site would further stabilize the above interactions and hence the observed p300HD inhibition. Other part(s) in the structure of the three inhibitors might be responsible for binding to another site (i.e., second binding site).

**Characterization of the Site of Molecular Interaction of p300HD with HAT Inhibitors.** To further verify the characteristic binding of nonspecific (garcinol and IG) versus specific (**1**) inhibitors to the enzyme and the above proposed mechanism of the HAT inhibition, an isobologram analysis was performed[29] (Figure 6). A concentration matrix of two compounds, IG versus garcinol (Figure 6a, left) and IG versus **1** (Figure 6a, right), was examined to determine whether the combination was

antagonistic, additive or synergistic. IG was taken as a common inhibitor in both of the matrixes, as the structure of IG closely resembles those of garcinol and **1**. In both cases, the compound combination resulted in an additive effect, consistent with the hypothesis that both molecules of garcinol and IG bind to the same site on p300HD and that a second binding site exists on the p300HD, to which probably one molecule of each garcinol, IG, and **1** binds (Figure 6). The above observation correlates positively with the logic that structurally very similar molecules interact with a similar region on the protein or receptor.

Further, in the absence of the 3D X-ray crystal structure of IG, the following computational strategy was adopted to obtain the optimized geometry of IG based on **1** due to the structural similarity. The structure of **1** (depository number CCDC645420) as obtained from the crystallographic data,[24] was optimized to get rid of any unnatural structural constrains. Following this, $-OCH_3$ was replaced by $-OH$ to construct the initial geometry of IG. In Supporting Information Figure S1, middle row in both top and bottom parts, we present the optimized geometry of IG. All the above calculations were performed using Gaussian 03 suite of programs as mentioned in methods section.[30] It is noted that 3D geometries (i.e., the spatial arrangement of atoms) of both IG and **1** are very similar and they mainly differ at the above-mentioned side group; $-OH$ is present in IG at the C-14 position, while $-OCH_3$ in **1** is at the same position (Supporting Information Figure S1; see middle and the rightmost parts in both rows). Further, we performed molecular docking of all the three inhibitors onto the crystal structure of p300HD[19] using Hex 4.5 software[31] (Figure 7). Significantly, an identical binding site was found for both garcinol and IG (Figure 7, top rows in the middle and the bottom column) which overlaps with acetyl-CoA binding site. In addition to this site, a second binding site also exists to which one molecule of each **1**, garcinol, and IG could be docked (Figure 7, lower rows in the middle and the last column) (see Supporting Information Table 1 for the putative HAT inhibitor interacting residues). These observations further support the above hypothesis and provide clues regarding the nature of the second binding site. It appears that the second binding site is present close to the proposed site of acetylation reaction[19] (Figure 7; see blown up images at the bottom and Supporting Information Table 1). It is noted that the docking studies have been done using the p300HD structure[19] lacking the autoinhibitory autoacetylation loop,[17,20] which has been proposed to fold back in cis and block the protein substrate binding at this site.[19] The kinetic studies suggest a noncompetitive mode of inhibition at the histone binding site for all three inhibitors, and the native protein has the autoinhibitory loop present that led us to speculate that the HAT inhibitors could be positively affecting the loop movement at this site which would further block the substrate binding and hence mediate its HAT inhibitory function.

To further support our hypothesis and to test our docking model, we selected four different amino acids on the p3000HD, S1396, Y1397, G1626, and R1627, which we predicted to make contacts with the inhibitors (e.g., **1**) at the proposed second binding site (Figure 7, blown up image at the bottom, and Supporting Information Table 1). We performed single amino acid mutagenesis on the mentioned residues S1396A, Y1397F, G1626A, and R1627K. All the mutants were active and were further used for the inhibition assay using the p300 specific inhibitor **1**. Interestingly, **1** failed to inhibit the HAT activity of all four mutant p300HD even at 100 $\mu$M (Figure 8). Taken together, these data support the existence of a second binding

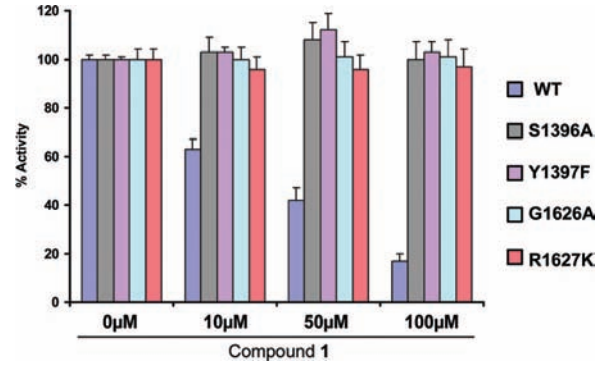


**Figure 8.** Mutagenesis study showing the percent inhibition of different putative **1** binding p300HD mutants. HAT inhibition assays were performed using 10, 50, and 100 $\mu$M **1**.

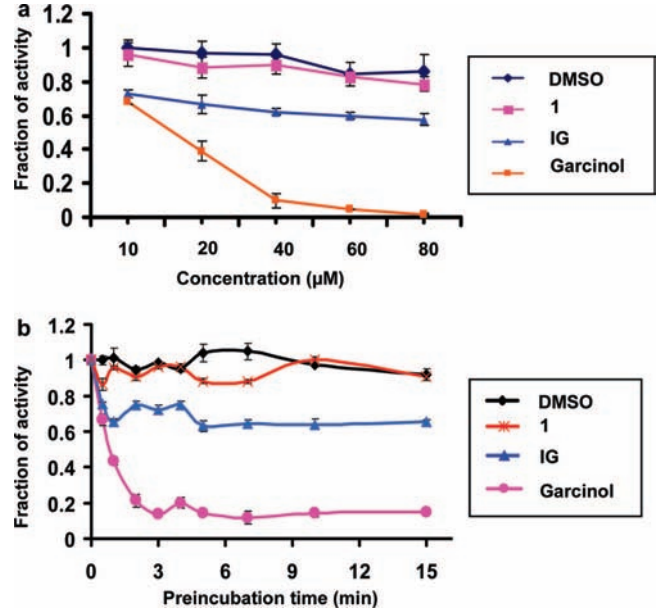


**Figure 9.** (a) Concentration dependent inhibition of PCAF HAT activity by different HAT inhibitors. HAT assays were performed in triplicate by using highly purified HeLa core histones. (b) Time course of the inactivation of PCAF in the presence of different HAT inhibitors at a constant concentration (10 $\mu$M). HAT assays were performed in triplicate by using highly purified HeLa core histones. Data are plotted as the fractional activity in both assays.

site close to the proposed site of the acetylation reaction[19] where **1** binds specifically.

**Effect of Garcinol and Its Derivative on PCAF Stability.** The high degree of p300 selectivity of **1** is unexpected, as all three inhibitors are very closely related to their structures and possess the hydrogen donors and acceptors. In order to understand the basis for the activity and selectivity of these polyisoprenylated benzophenones to p300 with respect to PCAF, we performed filter binding assays with increasing concentrations of HAT inhibitors (Figure 9a). As reported earlier,[24] **1** does not inhibit the PCAF HAT activity up to 80 $\mu$M (compare DMSO treated vs **1** of Figure 9a), while garcinol could inhibit around 90% of the PCAF HAT activity at 40 $\mu$M (Figure 9a; compare DMSO vs garcinol treated). Interestingly, IG, which also inhibits PCAF HAT activity, can only inhibit up to 50% at the highest concentration tested (compare DMSO vs IG treated of Figure 9a). These observations led us to suggest that molecular cyclization of garcinol to IG and **1** plays an important role in introducing the selectivity toward p300 by not allowing

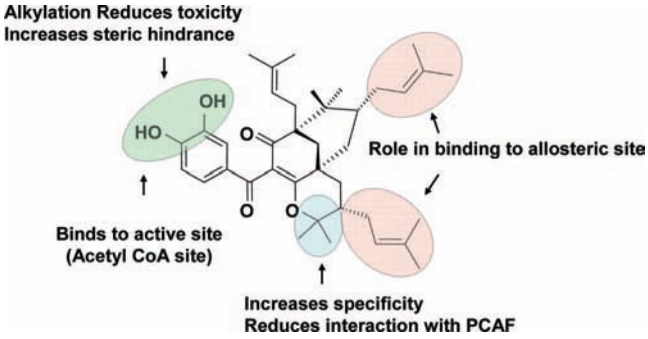


**Figure 10.** Summary of SAR for p300 HAT inhibitors. Arrows indicates the position and nature of each substitution tested in biochemical and biophysical studies.

**1** to interact with PCAF efficiently and thereby inhibiting the HAT activity.

Earlier work on PCAF has shown that it is an unstable enzyme that under commonly used assay conditions is rapidly and irreversibly inactivated.[32] Stabilization of PCAF requires its cofactor acetyl-CoA. We have shown that nonspecific inhibitor garcinol inhibits the PCAF HAT activity more potently than that of p300.[23] This led us to hypothesize that garcinol could be mediating its PCAF HAT inhibitory activity by destabilizing the enzyme irreversibly. Examination of the time course of inactivation (Figure 9b) revealed that 2 min of preincubation of PCAF with garcinol (10 $\mu$M) in the absence of acetyl-CoA is sufficient to bring down the enzyme activity by 80%. In contrast, no significant loss of enzymatic activity was observed under similar conditions in the presence of **1** compared to the DMSO solvent control. As expected and suggested above, the molecular cyclization of the nonspecific HAT inhibitor IG can inactivate the PCAF HAT activity only up to 50% even after 15 min of preincubation. These observations are in agreement with the above made conclusion that molecular cyclization has a role to play in creating specificity toward p300. In order to strengthen our above made observations, we performed molecular docking of all three inhibitors onto the crystal structure of PCAF HAT domain **(**PDB code 1CM0**)**.[27] Surprisingly, **1** was unable to make any hydrogen bonding with the PCAF HAT domain, whereas the very similar molecule IG can make one hydrogen bond with the residue T587, and garcinol can make two hydrogen bonds with the D610 of the PCAF HAT domain (Supporting Information Figure S3). Hence, these data suggest that indeed molecular cyclization restricts the ligands to interact properly with the PCAF, which results in poor PCAF inhibitory activity of **1** and IG as shown above. At the same time it also makes garcinol a potent PCAF inhibitor.

## Conclusion

Structure−activity relationships (SARs) obtained from our studies are summarized in Figure 10. The present study suggests that garcinol and **1** induce alteration in the secondary structure of the protein. Such alteration in the case of garcinol may be confined to the ordered segment of the protein. In contrast, **1** induces an alteration in the tertiary structure. It also stands out in exhibiting noncompetitive inhibition kinetics for both acetyl-CoA and histone substrates. The binding stochiometry of one **1** per complex with p300HD further implies that there is a high affinity enthalpy driven binding site in the p300HD for **1**. Binding to this site culminates in the noncompetitive inhibition for both acetyl-CoA and histone. Our data suggest that the binding site overlaps with the second binding site for garcinol and IG in the protein, which was also confirmed using p300HD mutants that totally abrogate the **1** interaction with the p300HD. However, the present data also emphasize the role of C-13 and C-14 −OH groups in garcinol and IG in their recognition of the acetyl-CoA binding site. The three-dimensional structures of the three ligands show that garcinol differs from the other two in the orientation of the blue circled moieties (Figure 1b and Supporting Information Figure S1). It further corroborates the proposition that the aromatic ring in garcinol and IG is required for the specific recognition of the acetyl-CoA binding site. On the other hand, the circled nonaromatic moieties are responsible for the noncompetitive inhibition for the histone substrate. Remarkably, p300HD cannot accommodate the bulky group of **1** at the acetyl-CoA binding site, which showed low structural tolerance at the acetyl-CoA binding site which is in contrast to the observed broad sequence selectivity,[19] i.e., higher structural tolerance at the other active site (protein binding site) for protein substrate. Hence, binding of HAT inhibitors (especially **1**) to the proposed highly electronegative site may be a useful tool to further elucidate the role of the acetylation reaction in the context of the p300 autoinhibitory loop movement. Our data further suggest that cyclization of garcinol leading to the formation of a lactone ring present in IG and **1** does not play a role in the recognition of p300HD. On the other hand, it has a role in imparting specificity toward p300 by not allowing HAT inhibitors to interact with PCAF. It might reduce the in vivo oxidation, thereby reducing the possibility of a toxic quinone type metabolic intermediate.[33] Thus, IG and **1** have better therapeutic potential.

**Significance.** The combination of biochemical, biophysical, and in vitro binding assays elucidates the mechanisms of p300 HAT inhibition and also demonstrates that the molecular scaffold of **1** is a potentially promising scaffold for further elaboration to obtain potent and specific p300 inhibitors. It may serve as a useful mechanistic probe to understand the role of the master regulator p300. Further, these data could also be useful for designing p300 (HAT) targeted therapeutics for AIDS, cancer, cardiac hypertrophy, and diabetes.

## Experimental Section

**Purification and Characterization of Garcinol and Its Derivatives.** Isolation, purification, and characterization of garcinol and synthesis of IG and **1** were done as described previously.[23,24]

**Purification of Bacterial Expressed p300 HAT Domain (p300HD).** 6His-tagged p300 HAT domain (aa 1284−1673) was purified from cells co-transformed with p300 HAT domain and SirT2 construct in *E. coli* BL21 (DE3) as described previously.[17−22] The 6His-tagged p300 HAT domain was affinity purified through the Ni-NTA column (Novagen) after a stepwise washing with up to 1 M NaCl. Bound proteins were eluted with 250 mM imidazole along with 100 mM NaCl. Fractions containing p300HD were pooled and dialyzed against the BC100 buffer (20 mM Tris-HCl [pH 7.9], 100 mM KCl, 20% glycerol, 0.1 mM DTT). For biophysical studies p300HD was further dialyzed against 20 mM Tris-HCl of pH 7.5, 0.2 mM EDTA, and 100 mM KCl. HAT assays were performed to check the enzyme activity before any in vitro study.

**Site-Directed Mutagenesis (SDM) of p300HD.** SDM was done to obtain different p300HD point mutants S1396A, Y1397F, G1626A, and R1627K. p300HD expression clone was used as the template, and the mutagenesis was done by the STRATAGENE SDM kit according to manufacturer's instructions. The positive clones were confirmed by sequencing and transformed

into the BL21 strain of *E.coli*. The expression and purification of the mutant proteins were done as mentioned above. All the mutants were enzymatically active as confirmed by filter binding assay.

**Determination of the Specific Activity of the p300HD.** Approximately 3.0 units/mg total protein was used. An amount of 1 unit is defined as the transfer of 1 nmol of [$^3$H]-acetate/min to the HeLa core histones. p300 full length samples with similar specific activity were used earlier and were in comparable range with p300HD. HAT assays were performed to determine the specific activity.

**Purification of Human Core Histones.** Human core histones were purified from HeLa nuclear pellet as described previously.[37] Protein was analyzed by 15% (w/v) SDS−PAGE (Supporting Information Figure S4).

**Histone Acetyltransferase Assay.** HAT gel fluorography/autoradiography assays were performed as previously reported.[23]

For kinetic analysis of HAT inhibitors' mediated inhibition of p300HD, filter binding assays were performed in the presence (1 and 5 $\mu$M) of garcinol and IG and (10 and 20 $\mu$M) of **1** or in the absence of these inhibitors. Of the two substrates, core histones and the acetyl group donor tritiated acetyl-CoA, the concentration of one substrate was kept constant and the other was varied. Concentration of core histones was kept constant at 1.6 $\mu$M, and $^3$H-acetyl-CoA was varied from 1.08 to 8.66 $\mu$M in the first assay. H$^3$-acetyl-CoA was kept constant at 2.78 $\mu$M, and core histones was varied from 0.003 to 0.068 $\mu$M in the second assay. The incorporation of the radioactivity was taken as a measure of the reaction velocity recorded as counts per minute (cpm). Each experiment was performed three times, and reproducibility was within 15%. Weighted averages of the values obtained were plotted as a lineweaver burk plot using Graphpad Prism software. The slope and intercept were replotted from the primary inhibition kinetic data to evaluate the inhibition constant, $K_i$.

**Absorbance and Fluorescence Measurement.** Absorption spectra were recorded with CECIL 7500 spectrophotometer. Fluorescence measurements were performed with a PerkinElmer LS55 luminescence spectrometer using 1 cm path length quartz cuvettes. Excitation and emission slits with a band-pass of 10 nm each were used for all measurements. During fluorescence measurements, the absorbance of the samples did not exceed 0.05 at 295 nm. Therefore, no correction for the optical filtering effect was done.

**Binding Analysis.** Results from fluorometric titrations were analyzed by the following method. The apparent dissociation constant ($K_d$) was determined using a nonlinear curve fitting analysis (eqs 1 and 2). Experimental points for the binding isotherm were fitted by the least-squares method.[36]

$$K_d = [C_p - (\Delta F/\Delta F_{max})C_p][C_1 - (\Delta F/\Delta F_{max})C_p]/[(\Delta F/\Delta F_{max})C_p] \quad (1)$$

$$C_p(\Delta F/\Delta F_{max})^2 - (C_p + C_1 + K_d)(\Delta F/\Delta F_{max}) + C_1 = 0 \quad (2)$$

where $\Delta F$ is the change in fluorescence emission intensity at 340 nm ($\lambda_{ex}$ = 295 nm) for each point of titration curve, $\Delta F_{max}$ is the same parameter when the protein is totally bound to the ligand (HATi), $C_l$ is the concentration of the HATi, and $C_p$ is the initial concentration of the protein. A double reciprocal plot of $1/\Delta F$ against $1/(C_p - C_l)$ was used for determination of $\Delta F_{max}$.

$$1/\Delta F = 1/\Delta F_{max} + K_d/[\Delta F_{max}(C_p - C_0)] \quad (3)$$

**Fluorescence Quenching Experiment.** Fluorescence quenching experiments were carried out by recording fluorescence intensities at 340 nm ($\lambda_{ex}$ = 295 nm) at 20 °C. Aliquots from a stock solution of a neutral quencher acrylamide were added successively to p300HD (1.2 $\mu$M) preincubated with 2.5 $\mu$M HATi for 2 min at room temperature in 20 mM Tris-HCl of pH 7.5, 0.2 mM EDTA, and 100 mM KCl. Quenching data were analyzed according to the Stern−Volmer equation[26] $F_0/F = 1 + K_{sv}[Q]$, where $F_o$ and $F$ are the initial and final fluorescence intensities, respectively, $K_{sv}$ is the quenching constant, and [Q] denotes the input concentration of acrylamide. A modified Stern−Volmer plot was also done to estimate the accessible ($f_e$) fraction of tryptophan residues according to the given equation

$$F_0/(F_0 - F) = 1/(K_{sv}f_e[Q]) + 1/f_e$$

**Circular Dichroism Spectroscopy.** Circular dichroism (CD) measurements were carried out in a JASCO J-810 spectropolarimeter (Jasco Corporation, Tokyo, Japan) at 20 °C equipped with a temperature controller. The CD scans were recorded for the wavelength range 200−250 nm at sensitivity set to 10 mdeg and scan speed 10 nm/min with a step size of 0.5 nm. The time constant was 8 s, and bandwidth was 2 nm. All measurements were carried out in a quartz cuvette of 1 mm path length in a reaction volume of 250 $\mu$L in 20 mM Tris-HCl of pH 7.5, 0.2 mM EDTA, and 100 mM KCl at 20 °C. In a reaction mixture containing 1.2 $\mu$M p300HD, individual titration for each HAT inhibitor was performed to achieve a concentration of 2.88 $\mu$M. The reaction mixture was incubated for 15 min prior to scanning. All spectra are the average of six runs. They are subtracted from appropriate buffer blank containing the ligands when required. They were smoothed within the permissible limits by the built-in software of the instrument.

**Isothermal Titration Calorimetry (ITC).** ITC experiments were carried out in a VP-ITC system (Microcal LLC) at 20 °C. Samples were centrifuged and degassed prior to titration. Titration of HAT inhibitors (HATi) against the protein (p300HD) was carried out by injecting 30−35 $\mu$M HATi in 20 mM Tris-HCl of pH 7.5, 0.2 mM EDTA, and 100 mM KCl buffer against 3 $\mu$M p300HD. A 2 min interval was allowed between injections for equilibration, sufficient for the return of the heat signal to baseline. A total of 35 injections were carried out to ensure complete titration. The protein concentration was chosen to achieve sufficiently high heat signals with a minimum enthalpy of dilution. To minimize the error associated with diffusion from the syringe during baseline equilibration, the first injection was only 1 $\mu$L and the associated small heat change was not considered for data analysis.

Blank experiments involving the titration of HATi against the buffer and the buffer against buffer were carried out and used for subtraction of the background heat change. The corrected heat change was plotted against molar ratio of the titrated products and analyzed using the manufacturer's software which yielded the stoichiometry $n$ (in terms of number of molecule of HATi/protein) and equilibrium constant ($K_a$). From the relationship $\Delta G° = -RT \ln K_a$ and the Gibbs−Helmholtz equation, the free energy of binding and the entropy of association ($\Delta S°$) were calculated.

**Isobologram Studies.** Isobologram analysis was performed as previously reported.[29]

The effect of the combination of IG versus garcinol and IG versus **1** was determined using the filter binding assays as described above. A concentration matrix of the two compounds was created and tested against p300HD. The % inhibition of core histone acetylation was determined at each of the combinations present in the matrix. The resulting isobologram was used to evaluate the effect of the combination. For the analysis, a plot in Cartesian coordinates of a dose combination that produces the same effect level is the basis for an isobologram. If two compounds have variable potency, a constant relative potency ($R$), which is the amount of compound needed to achieve the same fold activity (e.g., $IC_{50}$ for IG vs garcinol and $IC_{50}$ for IG vs **1**), is selected for the $X$ and $Y$ intercepts for isobologram analysis. The concentration of both compounds that corresponds to the respective $IC_{50}$ value is used as an intercept on both the $X$ and $Y$ axes. With these two intercepts, a theoretical line called the line of additivity is drawn between the two points. Experimental data obtained by the logarithmic titration of the two compounds mixed as a dose pair in a matrix that yields the same

effect level (IC value) are plotted on the isobologram. Statistical comparison of the line of additivity and the curve arising from experimental two drug dose combinations indicates if an effect is additive. Points falling below and above the line of additivity are subjected to regression analysis. Experimental data that are higher than the line of additivity are interpreted as antagonistic, and experimental data that are lower are interpreted as synergistic. Experimental data that fall on the line of additivity are considered additive.

**Molecular Calculation and Computational Strategy for IG Structure Optimization.** The Gaussian 03 program was used for all the ab inito molecular orbital calculations. Electron correlation was accounted for using the Becke's three-parameter hybrid method and the Lee−Yang−Parr correlation functional (B3LYP) at the 6-31+G (d) basis set.[35]

**Docking Studies.** The crystal structure of p300 HAT domain has been extracted from the PDB (PDB code 3BIY). The HAT domain was docked with the structure of garcinol (Pub Chem CID 5281560), IG, and **1** to find out their interaction sites on the HAT domain. Molecular simulation and the docking of p300HD with different HAT inhibitors were performed using Hex 4.5 software.[31] The docking calculations were done using 3D parametric functions of both the protein (p300HD) and the chemical structures (inhibitors), which were used to encode surface shape and electrostatic charge and potential distributions. The parametric functions are based on expansions of real orthogonal spherical polar basis functions. The docking was performed in full rotation mode; both domain and inhibitor were taken at 180 ranges for 20 000 solutions. The crystal structure of the PCAF HAT domain (PDB code 1CM0) is used to dock the HAT inhibitors using AutoDock 4 software (see Supporting Information Figure S 3).

**Acknowledgment.** We thank Dr. P. A. Cole for providing valuable reagents. We thank DBT, Government of India, and Jawaharlal Nehru Centre for Advanced Scientific Research (JNCASR) for financial assistance. M.A. is a CSIR Senior Research Fellow. We acknowledge Sairam Swaroop (T.S.U., JNCASR) for molecular calculation and computational strategy for IG structure optimization, and we acknowledge Sriram for initial help in molecular docking studies.

**Supporting Information Available:** Structures of p300HAT inhibitors and PCAF HAT domain, Stern−Volmer plots, purification profile, and listing of interacting residues. This material is available free of charge via the Internet at http://pubs.acs.org.

## References

(1) Richmond, T. J.; Davey, C. A. The structure of DNA in the nucleosome core. *Nature* **2003**, *423*, 145–150.
(2) Kim, M. Y.; Mauro, S.; Gevry, N.; Lis, J. T.; Kraus, W. L. NAD+-dependent modulation of chromatin structure and transcription by nucleosome binding properties of PARP-1. *Cell* **2004**, *119*, 803–814.
(3) Berger, S. L. Histone modifications in transcriptional regulation. *Curr. Opin. Genet. Dev.* **2002**, *12*, 142–148.
(4) Roth, S. Y.; Denu, J. M.; Allis, C. D. Histone acetyltransferases. *Annu. Rev. Biochem.* **2001**, *70*, 81–120.
(5) Swaminathan, V.; Reddy, B. A.; Ruthrotha Selvi, B.; Sukanya, M. S.; Kundu, T. K. Small molecule modulators in epigenetics: implications in gene expression and therapeutics. *Subcell. Biochem.* **2007**, *41*, 397–428.
(6) Marks, P. A.; Rifkind, R. A.; Richon, V. M.; Breslow, R.; Miller, T.; Kelly, W. K. Histone deacetylases and cancer: causes and therapies. *Nat. Rev. Cancer* **2001**, *1*, 194–202.
(7) Shikama, N.; Ivon, J.; La Thangue, N. The p300/CBP family: integrating signals with transcription factors and chromatin. *Trends Cell Biol.* **1997**, *7*, 230–236.
(8) Wolffe, A. P. Chromatin remodeling: Why it is important in cancer. *Oncogene* **2001**, *20*, 2988–2990.
(9) Rouaux, C.; Jokic, N.; Mbebi, C.; Boutillier, S.; Loeffler, J. P.; Boutillier, A. L. Critical loss of CBP/p300 histone acetylase activity by caspase-6 during neurodegeneration. *EMBO J.* **2003**, *22*, 6537–6549.
(10) Ogryzko, V. V.; Schiltz, R. L.; Russanova, V.; Howard, B. H.; Nakatani, Y. The transcriptional coactivators p300 and CBP are histone acetyltransferases. *Cell* **1996**, *87*, 953–959.
(11) Bannister, A. J.; Kouzarides, T. The CBP co-activator is a histone acetyltransferase. *Nature* **1996**, *384*, 641–643.
(12) Goodman, R. H.; Smolik, S. CBP/p300 in cell growth, transformation, and development. *Genes Dev.* **2000**, *14*, 1553–1577.
(13) Costanzo, A.; Merlo, P.; Pediconi, N.; Fulco, M.; Sartorelli, V.; Cole, P. A.; Fontemaggi, G.; Fanciulli, M.; Schiltz, L.; Blandino, G.; Balsano, C.; Levrero, M. DNA damage-dependent acetylation of p73 dictates the selective activation of apoptotic target genes. *Mol. Cell* **2002**, *9*, 175–186.
(14) Zhou, X. Y.; Shibusawa, N.; Naik, K.; Porras, D.; Temple, K.; Ou, H.; Kaihara, K.; Roe, M. W.; Brady, M. J.; Wondisford, F. E. Insulin regulation of hepatic gluconeogenesis through phosphorylation of CREB-binding protein. *Nat. Med.* **2004**, *10*, 633–637.
(15) Varier, R. A.; Kundu, T. K. Chromatin modifications (acetylation/deacetylation/methylation) as new targets for HIV therapy. *Curr. Pharm. Des.* **2006**, *12*, 1975–1993.
(16) Thompson, P. R.; Kurooka, H.; Nakatani, Y.; Cole, P. A. Transcriptional coactivator protein p300. Kinetic characterization of its histone acetyltransferase activity. *J. Biol. Chem.* **2001**, *276*, 33721–33729.
(17) Thompson, P. R.; Wang, D.; Wang, L.; Fulco, M.; Pediconi, N.; Zhang, D.; An, W.; Ge, Q.; Roeder, R. G.; Wong, J.; Levrero, M.; Sartorelli, V.; Cotter, R. J.; Cole, P. A. Regulation of the p300 HAT domain via a novel activation loop. *Nat. Struct. Mol. Biol.* **2004**, *11*, 308–315.
(18) Karanam, B.; Jiang, L.; Wang, L.; Kelleher, N. L.; Cole, P. A. Kinetic and mass spectrometric analysis of p300 histone acetyltransferase domain autoacetylation. *J. Biol. Chem.* **2006**, *281*, 40292–40301.
(19) Liu, X.; Wang, L.; Zhao, K.; Thompson, P. R.; Hwang, Y.; Marmorstein, R.; Cole, P. A. The structural basis of protein acetylation by the p300/CBP transcriptional coactivator. *Nature* **2008**, *451*, 846–850.
(20) Karanam, B.; Wang, L.; Wang, D.; Liu, X.; Marmorstein, R.; Cotter, R.; Cole, P. A. Multiple roles for acetylation in the interaction of p300 HAT with ATF-2. *Biochemistry* **2007**, *46*, 8207–8216.
(21) Black, J. C.; Choi, J. E.; Lombardo, S. R.; Carey, M. A mechanism for coordinating chromatin modification and preinitiation complex assembly. *Mol. Cell* **2006**, *23*, 809–818.
(22) Arif, M.; Kumar, G. V. P.; Narayana, C.; Kundu, T. K. Autoacetylation induced specific structural changes in histone acetyltransferase domain of p300: probed by surface enhanced Raman spectroscopy. *J. Phys. Chem. B* **2007**, *111*, 11877–11879.
(23) Balasubramanyam, K.; Altaf, M.; Varier, R. A.; Swaminathan, V.; Ravindran, A.; Sadhale, P. P.; Kundu, T. K. Polyisoprenylated benzophenone, garcinol, a natural histone acetyltransferase inhibitor, represses chromatin transcription and alters global gene expression. *J. Biol. Chem.* **2004**, *279*, 33716–33726.
(24) Mantelingu, K.; Reddy, B. A. A.; Swaminathan, V.; Kishore, A. H.; Siddappa, N. B.; Kumar, G. V. P.; Nagashankar, G.; Natesh, N.; Roy, S.; Sadhale, P. P.; Ranga, U.; Narayana, C.; Kundu, T. K. Specific inhibition of p300-HAT alters global gene expression and represses HIV replication. *Chem. Biol.* **2007**, *14*, 645–657.
(25) Majee, S.; Sen, R.; Guha, S.; Bhattacharya, D.; Dasgupta, D. Differential interactions of the $Mg^{2+}$ complexes of chromomycin A3 and mithramycin with poly(dG-dC) × poly(dC-dG) and poly(dG) × poly(dC). *Biochemistry* **1997**, *36*, 2291–2299.
(26) Lakowicz, R. J. *Principles of Fluorescence Spectroscopy*, 2nd ed.; Kluwer Academic/Plenum Publishers: New York, 1999; pp 242−249.
(27) Clements, A.; Rojas, J. R.; Trievel, R. C.; Wang, L.; Berger, S. L.; Marmorstein, R. Crystal structure of the histone acetyltransferase domain of the human PCAF transcriptional regulator bound to coenzyme A. *EMBO J.* **1999**, *18*, 3521–3532.
(28) Poux, A. N.; Cebrat, M.; Kim, C. M.; Cole, P. A.; Marmorstein, R. Structure of the GCN5 histone acetyltransferase bound to a bisubstrate inhibitor. *Proc. Natl. Acad. Sci. U.S.A.* **2002**, *99*, 14065–14070.
(29) Milne, J. C.; Lambert, P. D.; Schenk, S.; Carney, D. P.; Smith, J. J.; Gagne, D. J.; Jin, L.; Boss, O.; Perni, R. B.; Vu, C. B.; Bemis, J. E.; Xie, R.; Disch, J. S.; Ng, P. Y.; Nunes, J. J.; Lynch, A. V.; Yang, H.; Galonek, H.; Israelian, K.; Choy, W.; Iffland, A.; Lavu, S.; Medvedik, O.; Sinclair, D. A.; Olefsky, J. M.; Jirousek, M. R.; Elliott, P. J.; Westphal, C. H. Small molecule activators of SIRT1 as therapeutics for the treatment of type 2 diabetes. *Nature* **2007**, *450*, 712–716.
(30) Frisch, M. J.; Trucks, G. W.; Schlegel, H. B.; Scuseria, G. E.; Robb, M. A.; Cheeseman, J. R.; Montgomery, J. A., Jr.; Vreven, T.; Kudin, K. N.; Burant, J. C.; Millam, J. M.; Iyengar, S. S.; Tomasi, J.; Barone, V.; Mennucci, B.; Cossi, M.; Scalmani, G.; Rega, N.; Petersson, G. A.; Nakatsuji, H.; Hada, M.; Ehara, M.; Toyota, K.; Fukuda, R.; Hasegawa, J.; Ishida, M.; Nakajima, T.; Honda, Y.; Kitao, O.; Nakai, H.; Klene, M.; Li, X.; Knox, J. E.; Hratchian, H. P.; Cross, J. B.; Bakken, V.; Adamo, C.; Jaramillo, J.; Gomperts, R.; Stratmann, R. E.; Yazyev, O.; Austin, A. J.; Cammi, R.; Pomelli, C.; Ochterski, J. W.; Ayala, P. Y.; Morokuma, K.; Voth, G. A.; Salvador, P.; Dannenberg, J. J.; Zakrzewski, V. G.; Dapprich, S.; Daniels, A. D.; Strain, M. C.; Farkas,

O.; Malick, D. K.; Rabuck, A. D.; Raghavachari, K.; Foresman, J. B.; Ortiz, J. V.; Cui, Q.; Baboul, A. G.; Clifford, S.; Cioslowski, J.; Stefanov, B. B.; Liu, G.; Liashenko, A.; Piskorz, P.; Komaromi, I.; Martin, R. L.; Fox, D. J.; Keith, T.; Al-Laham, M. A.; Peng, C. Y.; Nanayakkara, A.; Challacombe, M.; Gill, P. M. W.; Johnson, B.; Chen, W.; Wong, M. W.; Gonzalez, C.; Pople, J. A. *Gaussian 03*, revision B.05; Gaussian, Inc.: Wallingford, CT, 2004.

(31) Mustard, D.; Ritchie, D. W. Docking essential dynamics eigenstructures. *Proteins: Struct., Funct., Bioinf.* **2005**, *60*, 269–274.

(32) Herrera, J. E.; Bergel, M.; Yang, X. J.; Nakatani, Y.; Bustin, M. The histone acetyltransferase activity of human GCN5 and PCAF is stabilized by coenzymes. *J. Biol. Chem.* **1997**, *272*, 27253–27258.

(33) Sarli, V.; Giannis, A. Selective inhibition of CBP/p300 HAT. *Chem Biol.* **2007**, *6*, 605–606.

(34) DeLano, W. L. *The PyMOL Molecular Graphics System*; DeLano Scientific LLC: Palo Alto, CA, 2002; http://www.pymol.org.

(35) (a) Becke, A. D. J. A new mixing of Hartree-Fock and local density-functional theories. *Chem. Phys.* **1993**, *98*, 1372–1377. (b) Lee, C.; Yang, W.; Parr, R. G. Development of the Colle−Salvetti correlation-energy formula into a functional of the electron density. *Phys. Rev. B* **1998**, *37*, 785–789 (B3LYP).

(36) Chakrabarty, S.; Roy, P.; Dasgupta, D. Interaction of the antitumor antibiotic chromomycin A3 with glutathione, a sulfhydryl agent, and the effect upon its DNA binding properties. *Biochem. Pharmacol.* **1998**, *31*, 3379–3386.

(37) Kundu, T. K.; Palthan, V. B.; Wang, Z.; An, W.; Cole, P. A.; Roeder, R. G. Activator-dependent transcription from chromatin in vitro involving targeted histone acetylation by p300. *Mol. Cell* **2000**, *6*, 551–561.

JM800657Z